

# Multi-scenario urban flood risk assessment by integrating future land use change models and hydrodynamic models

Qinke Sun<sup>1,2</sup>, Jiayi Fang<sup>1,2</sup>, Xuewei Dang<sup>3</sup>, Kepeng Xu<sup>1,2</sup>, Yongqiang Fang<sup>1,2</sup>, Xia Li<sup>1,2</sup>, Min Liu<sup>1,2</sup>

<sup>1</sup>School of Geographic Sciences, East China Normal University, Shanghai 200241, China

<sup>2</sup>Key Laboratory of Geographic Information Science (Ministry of Education), East China Normal University, Shanghai 200241, China

<sup>3</sup>Faculty of Geomatics, Lanzhou Jiaotong University, Lanzhou 730070, China

*Correspondence to:* Jiayi Fang (jyfang822@foxmail.com); Min Liu (mliu@geo.ecnu.edu.cn)

**Abstract.** Urbanization and climate change are the critical challenges in the 21<sup>st</sup> century. Flooding by extreme weather events and human activities can lead to catastrophic impacts in fast-urbanizing areas. However, high uncertainty in climate change and future urban growth limit the ability of cities to adapt to flood risk. This study presents a multi-scenario risk assessment method that couples the future land use simulation model (FLUS) and floodplain inundation model (LISFLOOD-FP) to simulate and evaluate the impacts of future urban growth scenarios with flooding under climate change (two representative concentration pathways (RCPs 2.6 and 8.5)). By taking coastal city of Shanghai as an example, we then quantify the role of urban planning policies in future urban development to compare urban development under multiple policy scenarios (Business as usual; Growth as planned; Growth as eco-constraints). Geospatial databases related to anthropogenic flood protection facilities, land subsidence, and storm surge are developed and used as inputs to the LISFLOOD-FP model to estimate flood risk under various urbanization and climate change scenarios. The results show that urban growth under the three scenario models manifests significant differences in expansion trajectories, influenced by key factors such as infrastructure development and policy constraints. Comparing the urban inundation results for the RCP2.6 and RCP8.5 scenarios, the urban inundation area under the growth as eco-constraints scenario is less than that under the business as usual scenario, but more than that under the growth as planned scenario. We also find that urbanization tends to expand more towards flood-prone areas under the restriction of ecological environment protection. The increasing flood risk information determined by model simulations help to understand the spatial distribution of future flood-prone urban areas and promote the re-formulation of urban planning in high-risk locations.

## 1 Introduction

Climate change and urbanization are the global challenges for the 21<sup>st</sup> century ( Ramaswami et al., 2016; Pecl et al., 2017). Floods have been key threats for many cities around the world driven by global climate change (Hallegatte et al., 2013; IPCC, 2014; Fang et al., 2020). Currently, more than 600 million people worldwide live in coastal cities that are less than 10 m

31 above sea level (United Nations, 2017). The United Nations reports that the global population living in cities is projected to  
32 reach 6.7 billion by 2050 (United Nations, 2018), especially in low elevation coastal areas, the population density is expected  
33 to be twice the current population density (Van Coppenolle and Temmerman, 2019), which means that the population of  
34 coastal cities will become increasingly concentrated in the future and impervious surfaces will become more numerous  
35 (Chen et al., 2020; He et al., 2021). On the other hand, the National Oceanic and Atmospheric Administration (NOAA)  
36 report suggests that global mean sea level will rise around 0.2 m to 2.0 m by 2100 under a continuing global warming trend  
37 (Parris et al., 2012). Additionally, properties and populations in many coastal areas will suffer more severely in the future if  
38 the effects of land subsidence are taken into account (Vousdoukas et al., 2018).

39 However, high uncertainty in flood risk and urban growth leads to a lack of capacity of cities to respond to the flooding  
40 arising from future climate change (Du et al., 2015; Tessler et al., 2015; Fang et al., 2021). Therefore, there is an urgent need  
41 for specialist knowledge and techniques to address the conflict between urbanization and flood risk (Wang et al., 2015; Lai  
42 et al., 2016; Bouwer, 2018; Haynes et al., 2018). Studies on urban flood risk assessment are more likely to simulate flood risk  
43 using different climate change scenarios or integrating different flood sources (Huong and Pathirana, 2013; Muis et al., 2015;  
44 Dullo et al., 2021). For example, Zhou et al. examine the impact of urban flood volumes and associated risks under RCP2.6  
45 and RCP8.5 scenarios (Zhou et al., 2019). Parodi et al. integrate the compound flood scenarios such as wave height, storm  
46 surge, and extreme sea level due to sea level rise to assess coastal flood risk (Parodi et al., 2020). However, ignoring the  
47 uncertainty of urban growth in urban flood risk assessment reduces the validity of the assessment (Gori et al., 2019), and  
48 hence an increased understanding of possible urban growth scenarios is needed, otherwise there is a lack of understanding of  
49 the consequences of future flooding (Zhao et al., 2017; Kim and Newman, 2020). Although there are some studies that have  
50 quantified future growth scenarios for urbanization (Nithila Devi et al., 2019; Lin et al., 2020), these studies have not  
51 considered the impact of existing planned policies that are designed to mitigate the impact of new development. In addition,  
52 the failure to integrate with broader climate change-related scenarios and possible extreme-case flood risks has led to  
53 underinvestment in climate adaptation actions by governments that do not well address the spatial consequences of future  
54 floods (Reckien et al., 2018; Berke et al., 2019). Thus, there is an urgent need to adopt a more comprehensive approach to  
55 assess the complexity of multiple possible scenarios of urbanization and dynamic flood risk in an integrated manner.

56 This paper uses the coupling of the future land use simulation model (FLUS) and the 2D floodplain inundation model  
57 (LISFLOOD-FP) to explore the possible interaction between different urbanization development scenarios and climate  
58 change scenarios. The FLUS model improves the simulation accuracy of the model by combining artificial neural network  
59 (ANN) and Cellular automata (CA) model to simulate nonlinear land use changes while considering parameters related to  
60 environment, society, climate change, etc. (Liu et al., 2017; Zhai et al., 2020). The LISFLOOD-FP model has become a  
61 mature hydrodynamic model that can predict potential flood events in near real-time and are widely used in engineering  
62 applications (Wing et al., 2019; Sosa et al., 2020). The coastal metropolitan Area of Shanghai in the Yangtze River Delta in  
63 China, one of the fastest urbanizing cities in the world, is used as a case study.

64 The paper asks, how different urban growth scenarios combined with climate change scenario analysis may help to inform  
65 preparedness for flood risks from climate change in urban flood risk assessments? To answer this question, we first assume  
66 some future simulation scenario by considering the factors that influence urban growth and lead to flood risk. Secondly, we  
67 coupled urban growth and flood risk scenarios and compared them using climate change scenarios from two representative  
68 concentrated pathways (RCP 2.6 and 8.5) proposed by the Intergovernmental Panel on Climate Change (IPCC). Finally, we  
69 assessed the risk of flooding in different urban development scenarios. The research illustrates the importance of assessing  
70 the performance of different future urban development scenarios in response to climate change, and the simulation study of  
71 urban risks will prove to decision-makers that incorporating disaster prevention measures into urban development plans will  
72 help to reduce disaster losses and improve the ability of urban systems to respond to floods.

73 The rest of paper is organized as follows: section 2 describes the characteristics of the study area and presents the data used  
74 in this paper; followed by a description of the methodology for integrating future land use change models and hydrodynamic  
75 models in Section 3. The results and discussion in Section 4 and Section 5. We divided the discussion section into two parts,  
76 on the one hand discussing the sources of uncertainty in the study, and the other part discussing adaptation policies for urban  
77 flood risk in the context of climate change. The conclusion of the study is described in Section 6.

## 78 **2 Study area and datasets**

### 79 **2.1 Study area**

80 As the alluvial plain of the Yangtze River Delta, Shanghai is located on the coast of the East China Sea between 30°40′–  
81 31°53′N and 120°52′–122°12′E, which borders the provinces of Jiangsu and Zhejiang to the West (Fig. 1). It's a typical  
82 middle latitude transition belt, marine land transitional zone and also a typical estuarine and coastal city with a fragile  
83 ecological environment. The land area of Shanghai is about 6340.50 km<sup>2</sup>, accounting for 0.06 % of the total area of China,  
84 and has 213 km of coastlines. The Shanghai metropolitan area has undergone rapid urban expansion in the past decades and  
85 has become one of the largest urban areas in the world in both size and population (Sun et al., 2020). However, Shanghai's  
86 topography is low, with an average elevation of 4 m above sea level, and there is no natural barrier against storm surges. In  
87 1905, one of the deadliest storm surges occurred in Shanghai, killing more than 29,000 people. Two years later, Typhoon  
88 Winnie made landfall in Shanghai, flooded more than 5,000 households (Du et al., 2020). Additionally, due to land  
89 subsidence and the increasing frequency and intensity of storm surges, Shanghai will become one of the most sensitive  
90 regions due to global climate change.

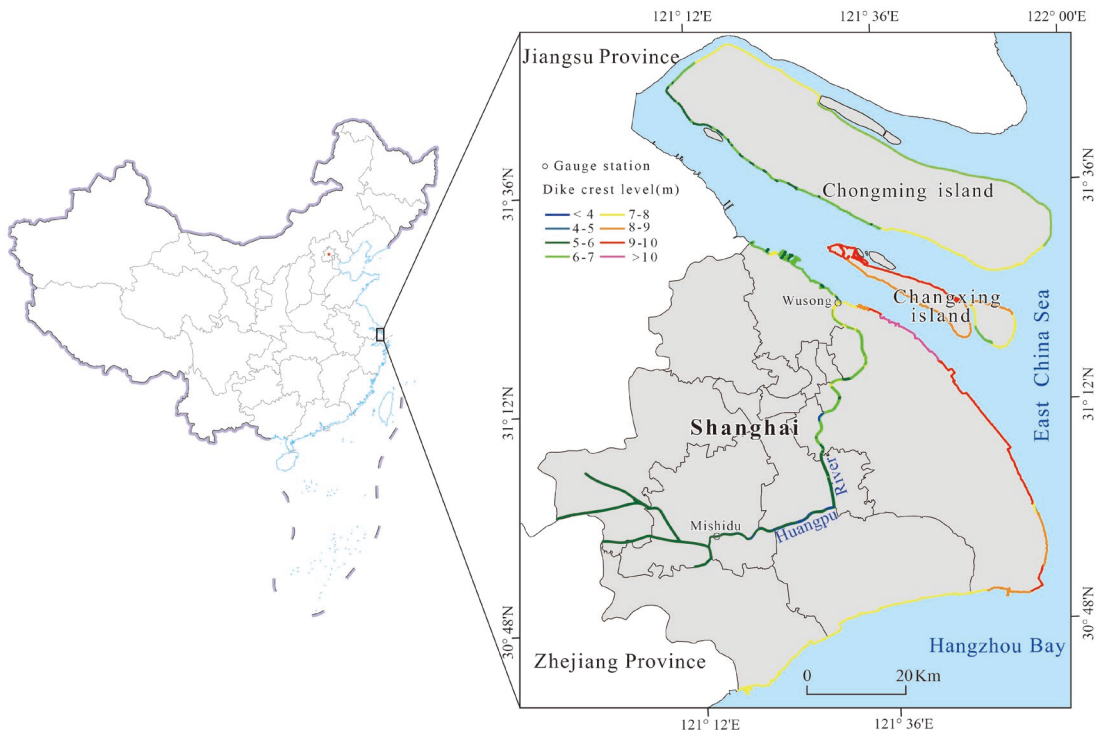


**Figure 1: Location map of the study area. The main inland rivers in Shanghai flow into the East China Sea through the Huangpu River. The line with coloured vectors in the figure indicates the different dike crest level in Shanghai.**

## 2.2 Data

The research used three main categories of data, including basic data, scenarios constraints data and flood simulation data (Table 1). The basic data include land use, topography, traffic network, traffic site, socio-economic data. The land use data with a resolution of 100 m×100 m from the Resource and Environmental Science and Data Center of the Chinese Academy of Sciences is currently the most accurate land use remote sensing monitoring data product in China (Liu et al., 2014). The data for 2005 and 2010 were derived from Landsat-TM/ETM remote sensing image data respectively, and the data for 2015 were interpreted using Landsat 8 remote sensing image. After the data were corrected and visually interpreted, the comprehensive evaluation accuracy of the interpretation accuracy of the first-class types of cultivated land, woodland, grassland, water area, urban land, and unused land reached more than 94.30 %, and the discrimination accuracy rate on the map patches reached 98.70 % (Xu et al., 2017). Within the allowable error range, it can be used as the basic data for analyzing land use changes.

Topography factors (DEM, slope), traffic network factors (distance to railway, highway, subway, and main roads), traffic site factors (distance to the city center, train station, and airports) and socio-economic factors (population, GDP), etc. as well as planning constraints, were determined to be spatial influence factors of the flood risk assessment of the Shanghai area.

108 The Advanced Spaceborne Thermal Emission and Reflection Radiometer (ASTER) digital elevation model (DEM), which  
109 has 30-meter resolution, served as the basis data for terrain heights and slopes. ASTER-DEM has been shown to be the most  
110 stable data performer among six types of open access DEM products (SRTM, ASTER-DEM, AW3D, MERIT, NASADEM  
111 and CoastalDEM) for flood inundation simulations with different return periods (Xu et al., 2021). Traffic network and site  
112 were collected from open-source data retrieved from OpenStreetMap (OSM) and POI data were extracted from Tencent Map.  
113 Euclidean distance was calculated for all vector data. The data of population and gross domestic product (GDP), were  
114 provided by the Resource and Environmental Science and Data Center of the Chinese Academy of Sciences (Xu, 2017a,  
115 2017b), and their time span was consistent with the land use data. According to the simulation forecast demand, all materials  
116 were converted into  $100 \times 100$  m grid by resampling. The spatial limiting factors were the basic ecological control line,  
117 permanent basic cropland and cultural protection control line as outlined in the 2017–2035 Shanghai City Master Plan. All  
118 the impact factor data were normalized, and the range of the value is between 0 and 1 to subsequent data mining.  
119 The storm surge data comes from the Global Tide and Surge Reanalysis (GTSR) dataset, which has been validated to have  
120 good accuracy (Muis et al., 2016). In addition, man-made flood defenses have been considered to reasonably evaluate the  
121 inundation impact of the flooding. The coastal flood protection data was obtained from the historical archival of the  
122 Shanghai Water Authority for Shanghai (Yin et al., 2020). All data sources are listed in in the table below.  
123 **Table 2. Data required and sources. The list details the resolution and sources of the data in the study.**

Category	Data Type	Resolution	Source
Basic data	Land use	100 m $\times$ 100m	Resource and Environmental Science and Data Center ( <a href="http://www.resdc.cn">http://www.resdc.cn</a> )
	Topography	Vector line	ASTER GDEM ( <a href="https://earthexplorer.usgs.gov/">https://earthexplorer.usgs.gov/</a> )
	Traffic network	Vector line	OpenStreetMap ( <a href="https://www.openstreetmap.org">https://www.openstreetmap.org</a> )
	Traffic site	Vector point	Tencent Map ( <a href="https://map.qq.com/">https://map.qq.com/</a> )
	Social economy	1 km $\times$ 1 km	Resource and Environmental Science and Data Center
Scenarios constraints	Ecological control line	Vector line	《2017-2035 Shanghai City Master Plan》
	Permanent basic cropland control line	Vector line	
	Cultural protection control line	Vector line	
Flood data	Floodwalls	Vector line	Shanghai Water Authority ( <a href="http://swj.sh.gov.cn/">http://swj.sh.gov.cn/</a> )
	Storm surge	Vector line	GTSR

124 **3 Methodology**

125 The presented approach for relative sea level rise scenario flood risk assessment is the integration of the FLUS model,  
126 LISFLOOD-FP model, and Markov chain model. In the framework, the FLUS model and Markov chain model are designed  
127 to stimulate complex land-use change processes in three different scenarios through 2030 to 2050, which include Business as  
128 usual (BU), Growth as planned (GP), Growth as eco-constraints (GE) scenarios. A Markov chain model is used to predict  
129 land-use demand in 2030 and 2050, combining planning policy factors, which is one of the crucial data inputs in the FLUS  
130 model. Next, the LISFLOOD-FP two-dimensional flood model is used to explore the potential flooding areas under the RCP  
131 2.6 and 8.5 scenarios in 2030 and 2050, to avoid the overestimation of the submerged range based on the GIS-based  
132 elevation area method. This model also considers the compound influence of sea-level rise, storm surge, and land subsidence.  
133 Finally, via ArcGIS spatial comprehensive analysis, the flooding of different land types is calculated employing different  
134 flooding scenarios. The overall flow chart of research is illustrated in Fig. 2.

135

136

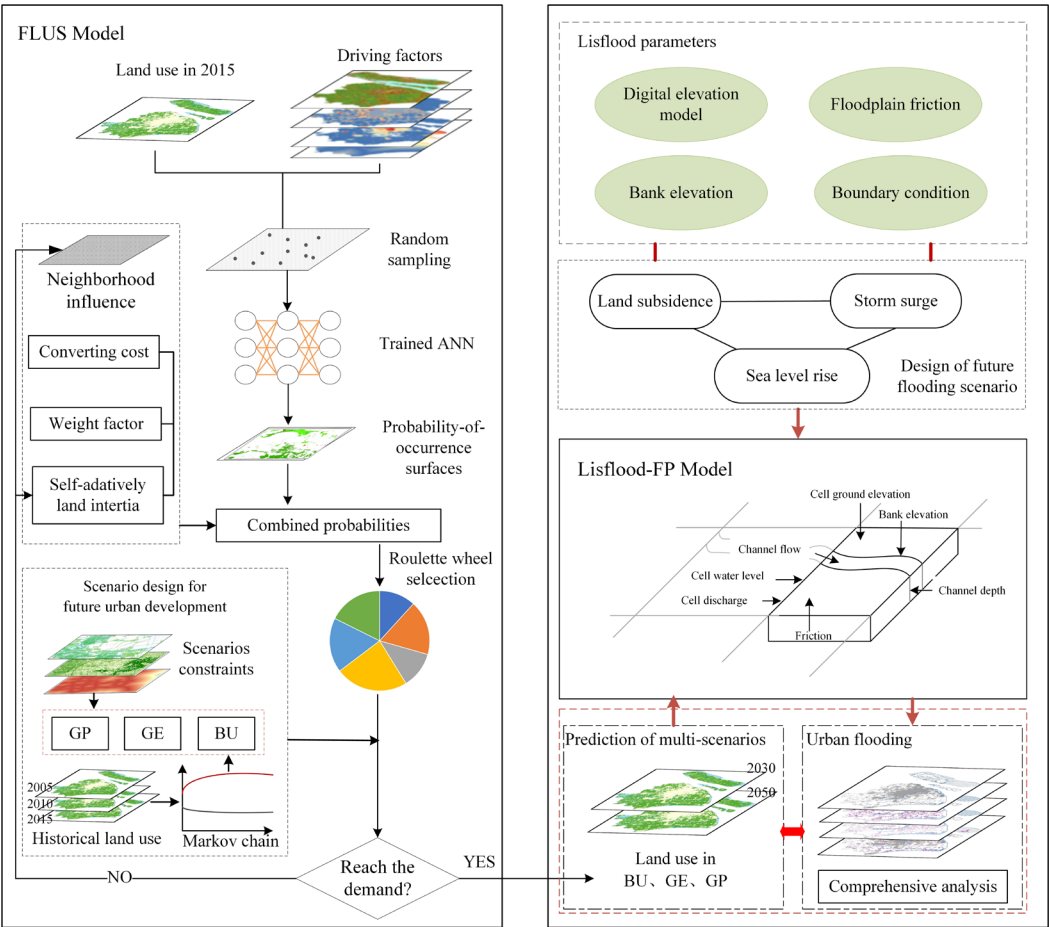


**Figure 2: The overall flow chart of research.**

### 137 3.1 Markov chain model

138 Markov chain model refers to the random transition process of state from one state to another, and its future state is only  
139 related to the state at previous moment. In the study of land use change, the type of land use at a certain moment is only  
140 related to the type of land use at the previous moment. Therefore, land-use change is a typical Markov process and has  
141 widely used in the prediction of land-use changes (Zhou et al., 2020). We predicted future land use by Eq. (1):

$$142 S_{(t+1)} = P_{i,j} \times S_t \quad (1)$$

143 where  $S_t$  and  $S_{t+1}$  represent the land use at times  $t$  and  $t+1$ , and  $P_{i,j}$  is a state transition matrix that land-use type  $i$  is  
144 converted to land-use type  $j$ . This model has a good predictive effect on the process state (Gounaridis et al., 2019). Therefore,  
145 we use the Markov chain to calculate the probability of the conversion of various land types, and then predict the number of  
146 future land changes.

### 147 3.2 The FLUS land use simulation model

148 The FLUS model is an upgraded version of a cellular automata model (Liu et al., 2017) which can solve the complex land  
149 use simulation problems by self-adaptive inertia and competition mechanism. The FLUS shows the highest current  
150 performances than other simulation models such as CLEU-S, SLEUTH, and LTM and has been applied to land use change  
151 simulation research at different scales and for different purposes (Liang et al., 2018; Lin et al., 2020).

152 As the most important scheme to manage the space of the urban area, an urban land use plan can reflect the general  
153 arrangement of land use in the future (Xu and Yang, 2019). In this research, three categories of urban growth scenarios are  
154 simulated through the FLUS model. The similarity of the three scenarios is that they use factors that affect urban  
155 development and changes, such as population, GDP, traffic, and slope, as the main spatial driving factors. The difference are  
156 as follows:

157 (i) Business as usual (BU): BU is natural growth without development laws and regulations. Its development is based on the  
158 premise of the current urban development patterns. Therefore, the land demand predicted by Markov is used as the constraint  
159 condition for the iteration of CA model in the subsequent application of the scenario.

160 (ii) Growth as planned (GP): Under the GP scenario, the urban growth projection that closely link to the master plan for  
161 Shanghai in terms of quantity, reflecting how the city government prefer to develop. The master plan requires that the total  
162 area of planned urban construction land does not exceed 3,200 km<sup>2</sup> in 2035. We choose an urban area of 2768 km<sup>2</sup> in 2030  
163 and 3200 km<sup>2</sup> in 2050 as the constraints under the GP scenario. The reason is that the Markov chain model projections result  
164 in an urban area is 2768 km<sup>2</sup> in 2030 and 3270 km<sup>2</sup> in 2050, and the total urban construction land area in 2035 of the  
165 Shanghai Master Plan does not exceed 3200 km<sup>2</sup>.

166 (iii) Growth as eco-constraints (GE): The GE scenario is an eco-environmental protection scenario which development is  
167 limited by the ecological environment protection. Combined with Shanghai's ecological and environmental protection

168 requirements and the distribution of permanent basic farmland, sensitive areas restricted for development are identified at the  
169 scenario, and we also establish a cultural protection control line for strengthening historical and cultural protection. In  
170 addition, the number of areas of future urban growth in the GE scenario also combines the requirements given in the urban  
171 master plan to enhance the reality of the scenario.

172 Therefore, the FLUS model is used to simulate future urban growth combining various scenarios. First, the driving factors  
173 and land-use data are trained by an ANN model to obtain a probability-of-occurrence map, and then incorporate with the  
174 self-adaptive land inertial, conversion cost, and neighborhood competition among the different land use types to estimate the  
175 combined probability for each grid. Next, combining the number of various types of land predicted by the Markov Chain  
176 model and considering the constraints of each scenario to predicted urban growth in 2030 and 2050. To better validate the  
177 model before predicting future change, we compared the output with the actual land use 2015. Note that the number of  
178 iterations in each scenario is set to 5000, which is much higher than the default value to show higher prediction accuracy.

### 179 **3.3 The LISFLOOD-FP flood inundation model**

180 LISFLOOD-FP is a 2D hydraulic model based on a raster grid (Bates et al., 2010), which can efficiently simulate the  
181 dynamic propagation of flood waves over fluvial and estuarine floodplains and show real-time changes in water depth of  
182 complex terrain. LISFLOOD-FP model solves the Saint-Venant equations at very low computational cost by omitting only  
183 the convective acceleration term over a structured grid using a highly efficient explicit finite difference scheme to produce a  
184 two-dimensional simulation of floodplain hydrodynamics (O’Loughlin et al., 2020). The model has been widely used in the  
185 applications of small-scale and large-scale urban waterlogging and flooding (Hoch et al., 2019; Rajib et al., 2020; Zhao et al.,  
186 2020).

187 In the present study, the LISFLOOD-FP model is used to simulate storm surge floods along the coast of Shanghai and floods  
188 along the Huangpu River. The effectiveness of the model in the study area has been verified by another article of our group  
189 members and shows good simulation results(Xu et al., 2021). In the boundary control of model, hydrological stations and  
190 global storm surge data are respectively employed as the input of the scenario design. However, Shanghai Geological  
191 Environmental Bulletin and land subsidence control plan show that land subsidence has a significant contribution to the  
192 flood hazards in Shanghai (Xian et al., 2018). Land subsidence in Shanghai is mainly caused by tectonic subsidence and  
193 compaction of sediments due to geological structure conditions and human activities. With reference to the long-term  
194 tectonic subsidence monitoring data of the very long baseline interferometer (VLBI) in the Sheshan bedrock and the land  
195 subsidence analysis rules of Yin et al. (Yin et al., 2013). therefore, the total land subsidence is predicted to be 0.12 m and  
196 0.24 m by 2030 and 2050, respectively. However, due to the uncertainty of future anthropogenic activities and spatial  
197 distribution, there could be large variations in the projection. This study also combines the storyline of future scenarios of the  
198 IPCC, namely the Representative Concentration Pathway (RCP) scenarios, and selects conservative (RCP2.6) and largest  
199 magnitude (RCP8.5) climate-change scenarios, with values from Kopp et al (Kopp et al., 2017). For the simulation of the  
200 Huangpu River flood, we conducted experiments for a 50-year return period under the RCP2.6 scenario and a 100-year

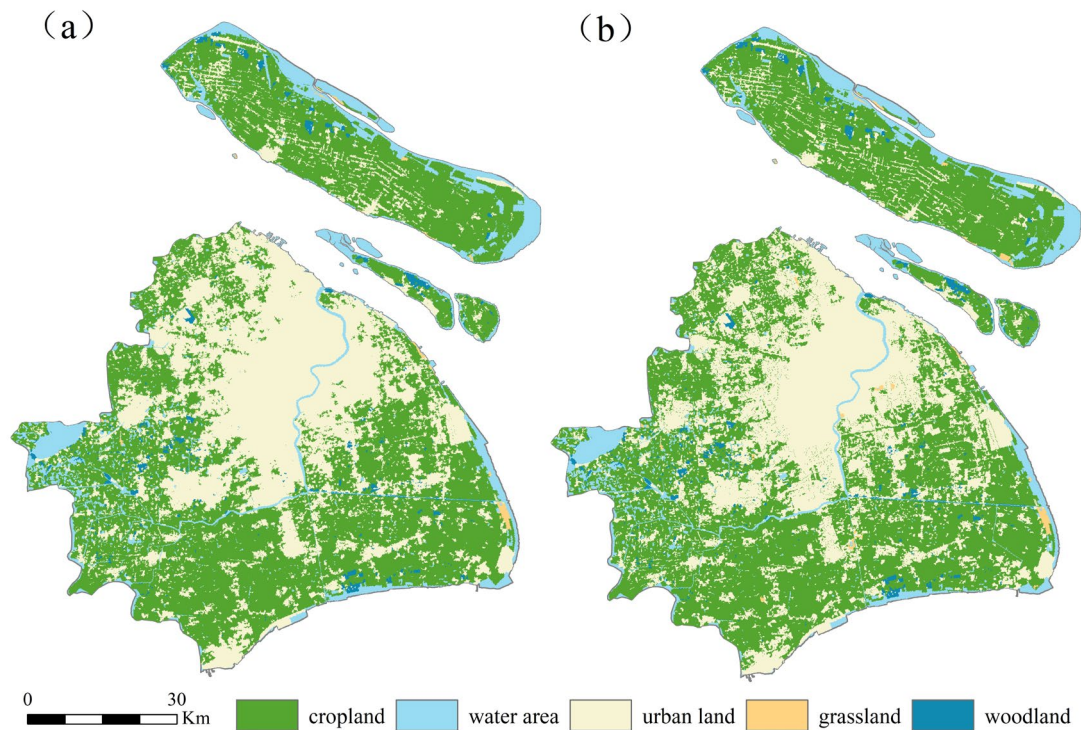


201 return period under the RCP8.5 scenario respectively during 2030 to 2050. For the 2030 and 2050, both Huangpu River and  
202 the coastal floods are following the RCP2.6 and RCP8.5 scenarios. Finally, we combine land subsidence and the RCP data to  
203 control the flood inundation simulation.

204 **4 Results**

205 **4.1 Model validity**

206 Model verification is the prerequisite for model operation, and the operation can only be carried out after confirming the  
207 model to be valid. The applicability of the proposed model was tested by simulating land use/cover changes (LUCC) in 2015  
208 at Shanghai. The spatial simulation result shows that the simulated result and the actual land use have a high consistency  
209 (Fig. 3). We compared the actual land use and the simulated result pixel by pixel in our study and found the overall accuracy  
210 (OA) was 93.20 %, the kappa coefficient (kappa) was 0.89. The discrepancy of the actual land use and simulated result is  
211 likely due to the neighborhood interaction in the CA model, in which grid cells in more urbanized neighborhoods have a  
212 higher probability to convert to urban, whereas the grid cells are less likely to change to urban in less urbanized  
213 neighborhoods. Overall, the measured model accuracy outputs showed an acceptable or good level of prediction, therefore  
214 the model is suitable for predicting changes in land use of the Shanghai area.



216 **Figure 3: Comparing the simulation results of Shanghai urban expansion with the actual situation, (a) simulation result in 2015; (b)**  
217 **actual land use in 2015.**

218 **4.2 Future land use changes**

219 Based on the conditions under three different development scenarios, we predicted the development of future urban land use  
220 change in 2030 and 2050. The prediction result shows different development patterns for each scenario (Fig. 4). Future urban  
221 growth under the BU scenario is primarily located in northwestern with some development in the central regions, and under  
222 the GP scenario the urban growth involves evenly distributed development. Urban growth in the GE scenario, however,  
223 Chongming Island regions have seen more urban growth, and the downtown area is not fully occupied by urban expansion  
224 due to restrictions.

225 Due to the impact of infrastructure construction, distance to the city center, and policy restrictions, Shanghai's overall urban  
226 expansion model shows a center-peripheral expansion. The built-up land areas in 2030 and 2050 are respectively projected to  
227 increase by about 6 % and 13 % as compared to 2015, the most significant reduction is found for cultivated land and  
228 woodland. Specifically, the built-up land areas in 2030 are respectively projected to increase by 427.32 km<sup>2</sup>, 428.27 km<sup>2</sup> and  
229 429.12 km<sup>2</sup> at BU, GP and GE scenarios, the built-up land areas in 2050 are respectively projected to increase by 926.38 km<sup>2</sup>,  
230 857.63 km<sup>2</sup> and 751.47 km<sup>2</sup> at BU, GP and GE scenarios. The most significant reduction is found for cropland, which is  
231 predicting in 2050 to decrease by 876.97 km<sup>2</sup>, 857.63 km<sup>2</sup> and 723.59 km<sup>2</sup> as compared to 2015 in BU, GP and GE scenarios.  
232 The southwestern region is not suitable for large-scale urban development, since large amounts of farmland in the region are  
233 listed as ecological protection areas, so the slow growth of these areas is not expected. The simulation maps show, as  
234 expected, land use changes under different planning scenarios, especially the urban sprawl trend at the GE scenario, creating  
235 new development areas in suburbs. To sum up, the urban expansion trajectory under BU, GP and GE shows significant  
236 differences, and these changes mainly at the expense of the cropland.

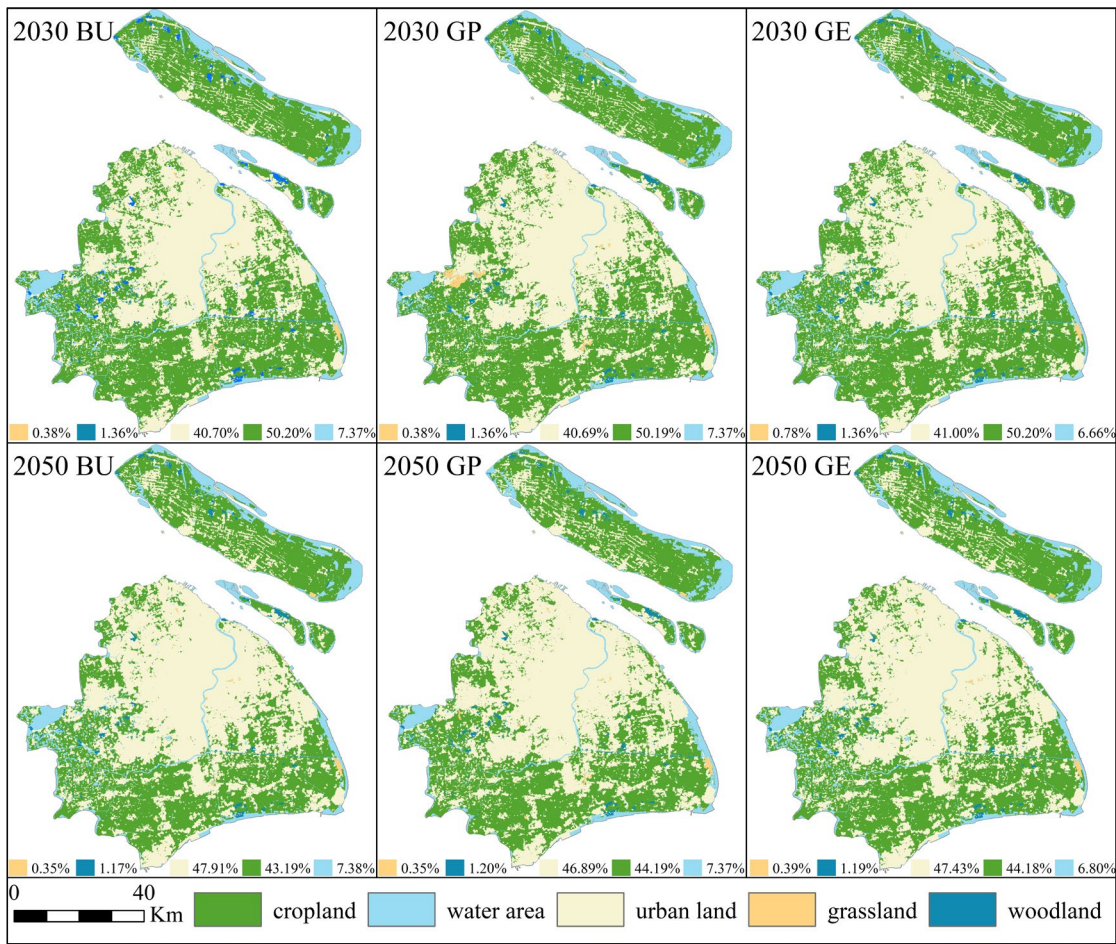


**Figure 4: Simulation results of different scenarios in 2030 (top) and 2050 (bottom). Each image shows the spatial distribution and the proportion of area of different land use types in the simulated scenario.**

### 4.3 Changing flood hazard in the future

The LISFLOOD-FP model is used to simulate the flood evolution process under RCP2.6 and RCP8.5 scenarios (the inundation results are plotted in Supplementary Figure 1), and then the submerged depth and area under different scenarios are statistically analyzed to explore the future flood risk under different RCP scenarios. First, the maximum water depth risk of the submerged area is counted, and the submerged area is divided into four depth levels: the submerged water depth is less than 0.5 m as shallow water area, water depth is 0.5-1 m as medium water area, the water depth is 1-2 m as deep water area, and submerged water depth is above 2 m as the extremely deep area. The area and proportion of each water depth level are calculated.

By comparing the scenarios in RCP2.6 and RCP8.5, it is evident that the submerged area is increasing with time (Table 2). The total flooded area increased by 162.43 km<sup>2</sup> and 189.44 km<sup>2</sup> under RCP2.6 and RCP8.5 scenarios from 2030 to 2050,

250 respectively. Additionally, the depth of submergence and the extent of submergence will gradually increase as the floodwater  
 251 spreads. Taking the area with submergence depth above 2 m as an example, under RCP2.6 scenario the area with  
 252 submergence is 353.69 km<sup>2</sup> and 401.57 km<sup>2</sup> respectively in 2030 and 2050, and under RCP8.5 scenario the area with  
 253 submergence is 356.28 km<sup>2</sup> and 418.36 km<sup>2</sup> respectively in 2030 and 2050. It shows that Shanghai will still face great flood  
 254 risk under these two scenarios.

255 **Table 2. Statistics of flood water depth.**

Category	<0.5 m		0.5-1 m		1-2 m		>2 m		Total /km <sup>2</sup>
	Area/ km <sup>2</sup>	Ratio/ %	Area/ km <sup>2</sup>	Ratio/ %	Area/ km <sup>2</sup>	Ratio/ %	Area/ km <sup>2</sup>	Ratio/ %	
2030 RCP2.6	138.61	14.54	164.07	17.21	296.98	31.15	353.69	37.10	953.35
2030 RCP8.5	137.13	14.23	169.76	17.61	300.82	31.21	356.28	36.96	963.99
2050 RCP2.6	125.04	11.21	229.81	20.60	359.36	32.21	401.57	35.99	1115.78
2050 RCP8.5	141.72	12.29	219.58	19.04	373.77	32.41	418.36	36.27	1153.43

256 **4.4 Future changes in urban flood risk**

257 The flood risk of the urban area is calculated by overlapping existing urban and projected future urban scenarios with future  
 258 flood risk zones. First, in the existing urban exposure to future flood risk scenarios (the upper left in Fig. 5), more urban  
 259 areas will be vulnerable to flood risk in the context of global climate change. The four pie charts for the EU scenarios  
 260 represent the proportion of the existing urban area affected by the future flood risk scenario. Under the RCP 2.6 scenario,  
 261 4.68 % and 5.96 % of the total existing urban areas in 2030 and 2050 would be susceptible to flood risk, respectively. In the  
 262 2030 and 2050 of the RCP8.5 scenarios the area of existing urban land which would be vulnerable to future flood risks are  
 263 110.27 km<sup>2</sup> and 146.23 km<sup>2</sup>, respectively. Many urban areas will be flooded under sea level rise caused by climate change  
 264 even when protected by levees, and more than 5 % of urban areas in Shanghai are still in the floodplain (Fig. 5).

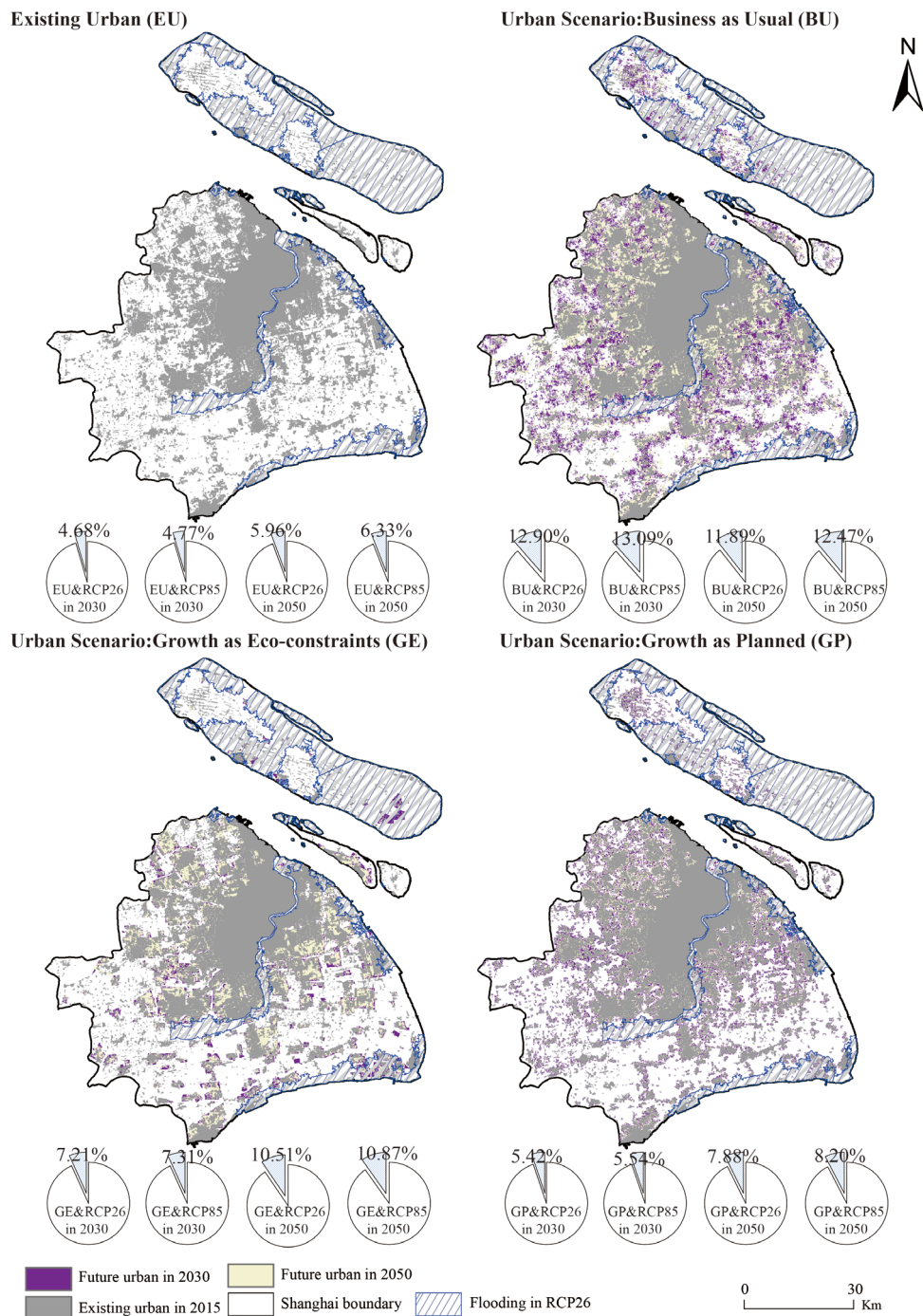


**Figure 5: Flood exposure of existing urban and future urban growth scenarios. The four pie charts for the BU, GE, and GP scenarios represent the proportion of new grown urban area exposed to flooding under the 2030 RCP2.6, 2030 RCP8.5, 2050 RCP2.6, and 2050 RCP8.5 scenarios, respectively. The four pie charts for the EU scenarios represent the proportion of the existing urban area affected by the future flood risk scenario.**



270 Future urban development would occur in the flood zone, with a rapid expansion of the urban area. Fig. 5 also shows the  
 271 comprehensive analysis results of the three urban growth scenarios under different climate change scenarios. Under the  
 272 RCP2.6 scenario, new growth in urban land area affected by flooding in 2030 are respectively 55.11 km<sup>2</sup>, 23.22 km<sup>2</sup>, and  
 273 30.92 km<sup>2</sup> at BU, GP and GE scenarios. Under the RCP8.5 scenario, future more urban growth areas would be affected by  
 274 the flooding, which will reach 115.53 km<sup>2</sup>, 70.36 km<sup>2</sup>, and 81.71 km<sup>2</sup> at BU, GP and GE scenarios in 2050, respectively. In  
 275 general, the higher the sea level rises, the greater the risk of flooding in future urban areas. Small changes in sea level rise  
 276 will affect a large amount of land, since the average altitude of Shanghai is only around 4 m.  
 277 **Table 3. Inundation of each land use type under different scenarios. The inundated areas of different land use types, including**  
 278 **cropland, woodland, grassland and urban land, were calculated for each scenario, where <sup>a</sup> indicates new grown areas of the urban**  
 279 **class affected by flooding.**

Time	Category	Urban scenario	Inundated areas (km <sup>2</sup> )			
			Cropland	Woodland	Grassland	Urban land <sup>a</sup>
2030	RCP2.6	BU	595.05	10.05	5.60	55.11
		GE	618.95	12.12	5.84	30.92
		GP	597.71	12.40	5.91	23.22
	RCP8.5	BU	602.38	10.23	5.67	55.92
		GE	625.97	12.29	5.91	31.23
		GP	604.32	12.59	5.98	23.72
2050	RCP2.6	BU	662.64	13.56	5.25	110.19
		GE	677.59	16.74	5.95	78.95
		GP	651.24	15.66	5.46	67.55
	RCP8.5	BU	683.56	15.06	5.70	115.53
		GE	698.98	18.05	6.40	81.71
		GP	672.30	16.85	5.91	70.36

280  
 281 The research found that the cultivated land is the most affected land type by flooding relative to urban areas, woodland and  
 282 grassland (Table 3). Under the GE scenario, the flooded area of cultivated land is 618.95 km<sup>2</sup> and 625.97 km<sup>2</sup> at the RCP2.6  
 283 and RCP8.5 in 2030, and 677.59 km<sup>2</sup> and 698.98 km<sup>2</sup> at the RCP2.6 and RCP8.5 in 2050. Further, the exposure of various  
 284 types of land is increasing with time, but urban land and cropland will be the most impacted land types in the future.  
 285 Comparing the three scenarios we can find that the urban development area under the planning scenario is less affected by

286 flooding, as compared to the business-as-usual development scenario. Comparing the inundation of the two planning  
287 scenarios (GE and GP), it also reflects the decision-makers' trade-off between economic development and ecological  
288 protection. The inundation area of the urban land under the GP scenario is less than that of the GE, which means that under  
289 the planning constraint of protecting ecological and cultural areas, urban built-up areas will develop on low-protection areas,  
290 which are more vulnerable to flooding. In conclusion, from reducing the risk of future flooding in urban areas, GE scenario  
291 shows to be better than BU scenario, but worse than GP scenario.

## 292 **5 Discussions**

### 293 **5.1 Source of uncertainties**

294 There are some limitations in our study, which is what we need to improve in the future. First, there is still more room to  
295 improve the accuracy of model prediction. In this study, the performance of the FLUS model is tested by kappa and OA  
296 measures, which shows a good range of prediction accuracy. In addition, this study proves that 16 driving factors contribute  
297 to the simulation and prediction of urban growth in Shanghai. The relationship between human and natural driving factors  
298 and land use change can be effectively integrated through the FLUS model embedded with an ANN, to obtain more realistic  
299 simulation results. However, if more influential drivers and the latest land cover are employed, the prediction would be  
300 having higher accuracy. Second, future flood risks in coastal areas are also not fully reflected through the use of  
301 hydrodynamic models, although it shows higher accuracy than the elevation area submergence method. On the one hand, this  
302 study is based on the modeling results of DEM data, which may overestimate or underestimate the simulation effect due to  
303 the error of DEM data. On the other hand, extreme storm surge and land subsidence data are combined to enhance the  
304 reliability of the extreme flood forecast in this study. However, the change of the impervious surface that affects hydrology  
305 is not yet considered in this study. When other land uses are converted to urban land uses, the risk of flooding will also  
306 greatly increase due to changes the of impervious surfaces. Therefore, it is necessary to dynamically adjust relevant factors  
307 affecting flood peak flows and risk in future forecasts to enhance the accuracy of prediction.

308 In the context of global climate change, extreme weather in the future may become more and more serious, so it is necessary  
309 to dynamically combine climate scenarios to develop more accurate flood risk delineation methods to guide urban planning  
310 in the future, and rely on new technology and equipment to provide data support. For example, unmanned aviation vehicles  
311 (UAVs) are deployed around the coastline to generate real-time information about weather conditions and sea-level changes  
312 (Cochrane et al., 2017). These tools will act as a complement to existing information and early warning systems, which also  
313 can provide guidance for coastal flood risk management and urban planning in the future. Overall, although uncertainty  
314 cannot be avoided when assessing coastal flood risk, the deviation of the proposed model output is within an acceptable  
315 range, which ensures the accuracy of coastal flood risk assessments.

316 **5.2 Recommendations on strategies and policies for urban adaptation to flooding**

317 In the twenty-first century, adapting to climate change and coastal flooding is a critical challenge for coastal cities. Human  
318 response to the impacts of flooding largely depends on the allocation of urban facilities and managers' planning for future  
319 urban development (Hunt and Watkiss, 2011). Shanghai is considered one of the most protected Chinese cities in terms of  
320 flood protection, yet it's the EAD/GDP (the Expected Annual Disruption, EAD), that is the direct damage to buildings and  
321 vehicles) ratio, which is as much as five times than in New York (Aerts et al., 2014). Therefore, there is an urgent need to  
322 adopt flood risk adaptation strategies in Shanghai.

323 We conducted a set of comparative experiments to analyze the coastal flood damage in Shanghai with and without flood  
324 walls (hard adaptation strategies). Our analysis considered the important effects of land subsidence and sea level rise on  
325 flood risk. We found that the current flood protection wall can reduce the flood losses due to climate change to a relatively  
326 low level (Supplementary Figure 2). In comparison, the flood protection wall constructed for the current conditions would  
327 reduce the flooded area under the RCP8.5 scenario by about 35 % and 36 % in 2030 and 2050, respectively. Furthermore,  
328 our results show that the area of future urban flood risk varies by scenario. Although the GE scenario performs higher than  
329 the GP scenario in terms of flood inundation area, this does not mean that the GE scenario is worse. From the cases of  
330 advanced flood risk management countries such as the Netherlands (Kabat et al., 2009; Song et al., 2018), an important  
331 success lesson for future flood protection design is to leave enough space along coasts for wetland migration and leave space  
332 for nature. In other words, "soft strategies" such as "working with rivers and nature" are considered in the flood protection  
333 measures. Therefore, from this perspective the GE scenario may be a more likely future development scenario among these  
334 three scenarios. Future, it is necessary to learn from the practical experience of advanced countries to strengthen the  
335 development and construction of coastal wetlands and tidal flat ecosystems, and further reduce the residual risk through the  
336 adaptive regulation of coastal ecosystems and other soft strategies. In addition, the implementation of "soft strategies" can  
337 increase the value of ecosystem services, increase biodiversity and carbon sequestration, and improve social welfare (Du et  
338 al., 2020).

339 **6 Conclusion**

340 Scenario-based assessment has been found to be a powerful approach in numerous flood risk studies. This study combines an  
341 urban growth model with a two-dimensional flood inundation model to not only simulate urban development dynamics more  
342 accurately, but also to discard the shortcomings of the traditional elevation inundation method of overestimating inundation  
343 areas. We have also tested the resilience of Shanghai to future different climate scenarios with the current flood wall. The  
344 results of the study are beneficial to local planners and coastal managers in making decisions of future protected areas and  
345 developments.

346 This study employed three urban development scenarios and detected the relationships of urbanization and climate changes  
347 in 2030 and 2050. The results of the study show that urban growth under the three scenario models manifests significant



348 differences in expansion trajectories, influenced by key factors such as infrastructure development and policy constraints.  
349 According to the predicted results of flood, new built-up areas are also potential vulnerable areas of flood risk. New built-up  
350 areas under different scenarios show significant vulnerability and exposure risk under different climate scenarios, even with  
351 the support of flood bank and other hard structures. Additionally, the research provided significant insights into the range  
352 and spatial distribution of flood risk in future urban areas.  
353 The current study is based on the multi scenario analysis of RCP global warming scenarios. In the future, the shared  
354 socioeconomic pathways (SSPs) can be combined to predict land use change, which make urban development scenarios  
355 more realistic choices. The results of this study estimate the future urban flood exposure areas, but this does not mean that all  
356 flood-vulnerable areas will be flooded, only that in these areas, the probability of each possible occurrence is greater.  
357 Therefore, proper preparations (such as definition restricted development zones) can reduce the damage risk of future flood  
358 and build more resilient cities.

359 **Author contributions**

360 Q. Sun and J. Fang designed the research; Q. Sun, K. Xu and X. Dang collected the data and carried out the experiments; Q.  
361 Sun wrote the draft; J. Fang, X. Dang, Y. Fang and M. Liu revised the manuscript; J. Fang, X. Li and M. Liu supervised and  
362 provided critical feedback. All authors contributed to the final version of the manuscript.

363 **Competing interests**

364 The authors declare that they have no conflict of interest.

365 **Funding source**

366 This work was supported by a grant from the National Natural Science Foundation of China (42001096, 41730646);  
367 Shanghai Sailing Program (19YF1413700); China Postdoctoral Science Foundation (2019M651429.); East China Normal  
368 University Institute of Belt and Road & Global Development (ECNU-BRGD-202106), and the National Key R&D Program  
369 of China (2017YFE0100700).

370 **References**

371 Aerts, J. C. J. H., Botzen, W. J. W., Emanuel, K., Lin, N., De Moel, H. and Michel-Kerjan, E. O.: Climate adaptation:  
372 Evaluating flood resilience strategies for coastal megacities, *Science* (80-. ), 344(6183), 473–475,  
373 doi:10.1126/science.1248222, 2014.

374 Bates, P. D., Horritt, M. S. and Fewtrell, T. J.: A simple inertial formulation of the shallow water equations for efficient two-  
375 dimensional flood inundation modelling, *J. Hydrol.*, 387(1–2), 33–45, doi:10.1016/j.jhydrol.2010.03.027, 2010.

376 Berke, P. R., Malecha, M. L., Yu, S., Lee, J. and Masterson, J. H.: Plan integration for resilience scorecard: evaluating  
377 networks of plans in six US coastal cities, *J. Environ. Plan. Manag.*, 62(5), 901–920,  
378 doi:10.1080/09640568.2018.1453354, 2019.

379 Bouwer, L. M.: Next-generation coastal risk models, *Nat. Clim. Chang.*, 8(9), 765–766, doi:10.1038/s41558-018-0262-2,  
380 2018.

381 Chen, G., Li, X., Liu, X., Chen, Y., Liang, X., Leng, J., Xu, X., Liao, W., Qiu, Y., Wu, Q. and Huang, K.: Global projections  
382 of future urban land expansion under shared socioeconomic pathways, *Nat. Commun.*, 11(1), 537, doi:10.1038/s41467-  
383 020-14386-x, 2020.

384 Cochrane, L., Cundill, G., Ludi, E., New, M., Nicholls, R. J., Wester, P., Cantin, B., Murali, K. S., Leone, M., Kituyi, E. and  
385 Landry, M. E.: A reflection on collaborative adaptation research in Africa and Asia, *Reg. Environ. Chang.*, 17(5), 1553–  
386 1561, doi:10.1007/s10113-017-1140-6, 2017.

387 Van Coppenolle, R. and Temmerman, S.: A global exploration of tidal wetland creation for nature-based flood risk  
388 mitigation in coastal cities, *Estuar. Coast. Shelf Sci.*, 226, 106262, doi:10.1016/j.ecss.2019.106262, 2019.

389 Du, S., Van Rompaey, A., Shi, P. and Wang, J.: A dual effect of urban expansion on flood risk in the Pearl River Delta  
390 (China) revealed by land-use scenarios and direct runoff simulation, *Nat. Hazards*, 77(1), 111–128,  
391 doi:10.1007/s11069-014-1583-8, 2015.

392 Du, S., Scussolini, P., Ward, P. J., Zhang, M., Wen, J., Wang, L., Koks, E., Diaz-Loaiza, A., Gao, J., Ke, Q. and Aerts, J. C.  
393 J. H.: Hard or soft flood adaptation? Advantages of a hybrid strategy for Shanghai, *Glob. Environ. Chang.*, 61, 102037,  
394 doi:https://doi.org/10.1016/j.gloenvcha.2020.102037, 2020.

395 Dullo, T. T., Darkwah, G. K., Gangrade, S., Morales-Hernández, M., Sharif, M. B., Kalyanapu, A. J., Kao, S. C., Ghafoor, S.  
396 and Ashfaq, M.: Assessing climate-change-induced flood risk in the Conasauga River watershed: An application of  
397 ensemble hydrodynamic inundation modeling, *Nat. Hazards Earth Syst. Sci.*, 21(6), 1739–1757, doi:10.5194/nhess-21-  
398 1739-2021, 2021.

399 Fang, J., Lincke, D., Brown, S., Nicholls, R. J., Wolff, C., Merkens, J. L., Hinkel, J., Vafeidis, A. T., Shi, P. and Liu, M.:  
400 Coastal flood risks in China through the 21st century – An application of DIVA, *Sci. Total Environ.*, 704, 135311,  
401 doi:10.1016/j.scitotenv.2019.135311, 2020.

402 Fang, J., Wahl, T., Zhang, Q., Muis, S., Hu, P., Fang, J., Du, S., Dou, T. and Shi, P.: Extreme sea levels along coastal China:  
403 uncertainties and implications, *Stoch. Environ. Res. Risk Assess.*, 35(2), 405–418, doi:10.1007/s00477-020-01964-0,  
404 2021.

405 Gori, A., Blessing, R., Juan, A., Brody, S. and Bedient, P.: Characterizing urbanization impacts on floodplain through  
406 integrated land use, hydrologic, and hydraulic modeling, *J. Hydrol.*, 568, 82–95, doi:10.1016/j.jhydrol.2018.10.053,  
407 2019.

408 Gounaridis, D., Chorianopoulos, I., Symeonakis, E. and Koukoulas, S.: A Random Forest-Cellular Automata modelling  
 409 approach to explore future land use/cover change in Attica (Greece), under different socio-economic realities and scales,  
 410 *Sci. Total Environ.*, 646, 320–335, doi:10.1016/j.scitotenv.2018.07.302, 2019.

411 Hallegatte, S., Green, C., Nicholls, R. J. and Corfee-Morlot, J.: Future flood losses in major coastal cities, *Nat. Clim. Chang.*,  
 412 3(9), 802–806, doi:10.1038/nclimate1979, 2013.

413 Haynes, P., Hehl-Lange, S. and Lange, E.: Mobile Augmented Reality for Flood Visualisation, *Environ. Model. Softw.*, 109,  
 414 380–389, doi:10.1016/j.envsoft.2018.05.012, 2018.

415 He, C., Liu, Z., Wu, J., Pan, X., Fang, Z., Li, J. and Bryan, B. A.: Future global urban water scarcity and potential solutions,  
 416 *Nat. Commun.*, 12(1), 1–11, doi:10.1038/s41467-021-25026-3, 2021.

417 Hoch, J. M., Eilander, D., Ikeuchi, H., Baart, F. and Winsemius, H. C.: Evaluating the impact of model complexity on flood  
 418 wave propagation and inundation extent with a hydrologic-hydrodynamic model coupling framework, *Nat. Hazards*  
 419 *Earth Syst. Sci.*, 19(8), 1723–1735, doi:10.5194/nhess-19-1723-2019, 2019.

420 Hunt, A. and Watkiss, P.: Climate change impacts and adaptation in cities: A review of the literature, *Clim. Change*, 104(1),  
 421 13–49, doi:10.1007/s10584-010-9975-6, 2011.

422 Huong, H. T. L. and Pathirana, A.: Urbanization and climate change impacts on future urban flooding in Can Tho city,  
 423 Vietnam, *Hydrol. Earth Syst. Sci.*, 17(1), 379–394, doi:10.5194/hess-17-379-2013, 2013.

424 IPCC: Climate Change 2014: Impacts, Adaptation, and Vulnerability. Part A: Global and Sectoral Aspects. Contribution of  
 425 Working Group II to the Fifth Assessment Report of the Intergovernmental Panel on Climate Change, Cambridge  
 426 University Press, Cambridge, UK., 2014.

427 Kabat, P., Fresco, L. O., Stive, M. J. F., Veerman, C. P., van Alphen, J. S. L. J., Parmet, B. W. A. H., Hazeleger, W. and  
 428 Katsman, C. A.: Dutch coasts in transition, *Nat. Geosci.*, 2(7), 450–452, doi:10.1038/ngeo572, 2009.

429 Kim, Y. and Newman, G.: Advancing scenario planning through integrating urban growth prediction with future flood risk  
 430 models, *Comput. Environ. Urban Syst.*, 82, 101498, doi:https://doi.org/10.1016/j.compenvurbsys.2020.101498, 2020.

431 Kopp, R. E., DeConto, R. M., Bader, D. A., Hay, C. C., Horton, R. M., Kulp, S., Oppenheimer, M., Pollard, D. and Strauss,  
 432 B. H.: Evolving understanding of Antarctic ice-sheet physics and ambiguity in probabilistic sea-level projections, *arXiv*,  
 433 2017.

434 Lai, C., Shao, Q., Chen, X., Wang, Z., Zhou, X., Yang, B. and Zhang, L.: Flood risk zoning using a rule mining based on ant  
 435 colony algorithm, *J. Hydrol.*, 542, 268–280, doi:https://doi.org/10.1016/j.jhydrol.2016.09.003, 2016.

436 Liang, X., Liu, X., Li, X., Chen, Y., Tian, H. and Yao, Y.: Delineating multi-scenario urban growth boundaries with a CA-  
 437 based FLUS model and morphological method, *Landsc. Urban Plan.*, 177, 47–63,  
 438 doi:10.1016/j.landurbplan.2018.04.016, 2018.

439 Lin, W., Sun, Y., Nijhuis, S. and Wang, Z.: Scenario-based flood risk assessment for urbanizing deltas using future land-use  
 440 simulation (FLUS): Guangzhou Metropolitan Area as a case study, *Sci. Total Environ.*, 739, 139899,  
 441 doi:10.1016/j.scitotenv.2020.139899, 2020.

442 Liu, J., Kuang, W., Zhang, Z., Xu, X., Qin, Y., Ning, J., Zhou, W., Zhang, S., Li, R., Yan, C., Wu, S., Shi, X., Jiang, N., Yu,  
 443 D., Pan, X. and Chi, W.: Spatiotemporal characteristics, patterns and causes of land use changes in China since the late  
 444 1980s, *Dili Xuebao/Acta Geogr. Sin.*, 69(1), 3–14, doi:10.11821/dlxb201401001, 2014.

445 Liu, X., Liang, X., Li, X., Xu, X., Ou, J., Chen, Y., Li, S., Wang, S. and Pei, F.: A future land use simulation model (FLUS)  
 446 for simulating multiple land use scenarios by coupling human and natural effects, *Landsc. Urban Plan.*, 168, 94–116,  
 447 doi:10.1016/j.landurbplan.2017.09.019, 2017.

448 Muis, S., Güneralp, B., Jongman, B., Aerts, J. C. J. H. and Ward, P. J.: Flood risk and adaptation strategies under climate  
 449 change and urban expansion: A probabilistic analysis using global data, *Sci. Total Environ.*, 538, 445–457,  
 450 doi:10.1016/j.scitotenv.2015.08.068, 2015.

451 Muis, S., Verlaan, M., Winsemius, H. C., Aerts, J. C. J. H. and Ward, P. J.: A global reanalysis of storm surges and extreme  
 452 sea levels, *Nat. Commun.*, 7, 11969, doi:10.1038/ncomms11969, 2016.

453 Nithila Devi, N., Sridharan, B. and Kuiry, S. N.: Impact of urban sprawl on future flooding in Chennai city, India, *J. Hydrol.*,  
 454 574, 486–496, doi:10.1016/j.jhydrol.2019.04.041, 2019.

455 O’Loughlin, F. E., Neal, J., Schumann, G. J. P., Beighley, E. and Bates, P. D.: A LISFLOOD-FP hydraulic model of the  
 456 middle reach of the Congo, *J. Hydrol.*, 580, doi:10.1016/j.jhydrol.2019.124203, 2020.

457 Parodi, M. U., Giardino, A., Van Dongeren, A., Pearson, S. G., Bricker, J. D. and Reniers, A. J. H. M.: Uncertainties in  
 458 coastal flood risk assessments in small island developing states, *Nat. Hazards Earth Syst. Sci.*, 20(9), 2397–2414,  
 459 doi:10.5194/nhess-20-2397-2020, 2020.

460 Parris, A., Bromirski, P., Burkett, V., Cayan, D., Culver, M., Hall, J., Horton, R., Knuuti, K., Moss, R., Obeysekera, J.,  
 461 Sallenger, A. and Weiss, J.: Global Sea Level Rise Scenarios for the US National Climate Assessment, NOAA Tech  
 462 Memo OAR CPO, 1–37, doi:https://scenarios.globalchange.gov/sites/default/files/NOAA\_SLR\_r3\_0.pdf, 2012.

463 Pecl, G. T., Araújo, M. B., Bell, J. D., Blanchard, J., Bonebrake, T. C., Chen, I. C., Clark, T. D., Colwell, R. K., Danielsen,  
 464 F., Evengård, B., Falconi, L., Ferrier, S., Frusher, S., Garcia, R. A., Griffis, R. B., Hobday, A. J., Janion-Scheepers, C.,  
 465 Jarzyna, M. A., Jennings, S., Lenoir, J., Linnetved, H. I., Martin, V. Y., McCormack, P. C., McDonald, J., Mitchell, N.  
 466 J., Mustonen, T., Pandolfi, J. M., Pettorelli, N., Popova, E., Robinson, S. A., Scheffers, B. R., Shaw, J. D., Sorte, C. J.  
 467 B., Strugnell, J. M., Sunday, J. M., Tuanmu, M. N., Vergés, A., Villanueva, C., Wernberg, T., Wapstra, E. and Williams,  
 468 S. E.: Biodiversity redistribution under climate change: Impacts on ecosystems and human well-being, *Science* (80-. ),  
 469 355(6332), doi:10.1126/science.aai9214, 2017.

470 Rajib, A., Liu, Z., Merwade, V., Tavakoly, A. A. and Follum, M. L.: Towards a large-scale locally relevant flood inundation  
 471 modeling framework using SWAT and LISFLOOD-FP, *J. Hydrol.*, 581, 124406, doi:10.1016/j.jhydrol.2019.124406,  
 472 2020.

473 Ramaswami, A., Russell, A. G., Culligan, P. J., Rahul Sharma, K. and Kumar, E.: Meta-principles for developing smart,  
 474 sustainable, and healthy cities, *Science* (80-. ), 352, 940–943, doi:10.1126/science.aaf7160, 2016.

475 Reckien, D., Salvia, M., Heidrich, O., Church, J. M., Pietrapertosa, F., De Gregorio-Hurtado, S., D'Alonzo, V., Foley, A.,  
 476 Simoes, S. G., Krkoška Lorencová, E., Orru, H., Orru, K., Wejs, A., Flacke, J., Olazabal, M., Geneletti, D., Feliu, E.,  
 477 Vasilie, S., Nador, C., Krook-Riekkola, A., Matosović, M., Fokaides, P. A., Ioannou, B. I., Flamos, A., Spyridaki, N. A.,  
 478 Balzan, M. V., Fülöp, O., Paspaldzhiev, I., Grafakos, S. and Dawson, R.: How are cities planning to respond to climate  
 479 change? Assessment of local climate plans from 885 cities in the EU-28, *J. Clean. Prod.*, 191, 207–219,  
 480 doi:10.1016/j.jclepro.2018.03.220, 2018.

481 Song, J., Fu, X., Wang, R., Peng, Z.-R. and Gu, Z.: Does planned retreat matter? Investigating land use change under the  
 482 impacts of flooding induced by sea level rise, *Mitig. Adapt. Strateg. Glob. Chang.*, 23(5), 703–733,  
 483 doi:10.1007/s11027-017-9756-x, 2018.

484 Sosa, J., Sampson, C., Smith, A., Neal, J. and Bates, P.: A toolbox to quickly prepare flood inundation models for  
 485 LISFLOOD-FP simulations, *Environ. Model. Softw.*, 123, 104561, doi:https://doi.org/10.1016/j.envsoft.2019.104561,  
 486 2020.

487 Sun, L., Chen, J., Li, Q. and Huang, D.: Dramatic uneven urbanization of large cities throughout the world in recent decades,  
 488 *Nat. Commun.*, 11(1), 5366, doi:10.1038/s41467-020-19158-1, 2020.

489 Tessler, Z. D., Vorosmarty, C. J., Grossberg, M., Gladkova, I., Aizenman, H., Syvitski, J. P. M. and Foufoula-Georgiou, E.:  
 490 Profiling risk and sustainability in coastal deltas of the world, *Science* (80-. ), 349, 638–643,  
 491 doi:10.1126/science.aab3574, 2015.

492 United Nations: Factsheet: People and oceans., 2017.

493 United Nations: 2018 Revision of World Urbanization Prospects. [online] Available from: <https://population.un.org/wup/>,  
 494 2018.

495 Vousdoukas, M. I., Mentaschi, L., Voukouvalas, E., Verlaan, M., Jevrejeva, S., Jackson, L. P. and Feyen, L.: Global  
 496 probabilistic projections of extreme sea levels show intensification of coastal flood hazard, *Nat. Commun.*, 9(1), 1–12,  
 497 doi:10.1038/s41467-018-04692-w, 2018.

498 Wang, Z., Lai, C., Chen, X., Yang, B., Zhao, S. and Bai, X.: Flood hazard risk assessment model based on random forest, *J.*  
 499 *Hydrol.*, 527, 1130–1141, doi:10.1016/j.jhydrol.2015.06.008, 2015.

500 Wing, O. E. J., Sampson, C. C., Bates, P. D., Quinn, N., Smith, A. M. and Neal, J. C.: A flood inundation forecast of  
 501 Hurricane Harvey using a continental-scale 2D hydrodynamic model, *J. Hydrol. X*, 4, 100039,  
 502 doi:https://doi.org/10.1016/j.hydroa.2019.100039, 2019.

503 Xian, S., Yin, J., Lin, N. and Oppenheimer, M.: Influence of risk factors and past events on flood resilience in coastal  
 504 megacities: Comparative analysis of NYC and Shanghai, *Sci. Total Environ.*, 610–611, 1251–1261,  
 505 doi:10.1016/j.scitotenv.2017.07.229, 2018.

506 Xu, K., Fang, J., Fang, Y., Sun, Q., Wu, C. and Liu, M.: The Importance of Digital Elevation Model Selection in Flood  
 507 Simulation and a Proposed Method to Reduce DEM Errors: A Case Study in Shanghai, *Int. J. Disaster Risk Sci.*,  
 508 doi:10.1007/s13753-021-00377-z, 2021.

509 Xu, W. (Ato) and Yang, L.: Evaluating the urban land use plan with transit accessibility, *Sustain. Cities Soc.*, 45, 474–485,  
 510 doi:10.1016/j.scs.2018.11.042, 2019.

511 Xu, X., Liu, J., Zhang, Z., Zhou, W., Zhang, S., Li, R., Yan, C., Wu, S. and Shi, X.: A Time Series Land Ecosystem  
 512 Classification Dataset of China in Five-Year Increments (1990–2010), *J. Glob. Chang. Data Discov.*, 1(1), 52–59,  
 513 doi:10.3974/geodp.2017.01.08, 2017.

514 Yin, J., Yu, D., Yin, Z., Wang, J. and Xu, S.: Modelling the combined impacts of sea-level rise and land subsidence on storm  
 515 tides induced flooding of the Huangpu River in Shanghai, China, *Clim. Change*, 119(3–4), 919–932,  
 516 doi:10.1007/s10584-013-0749-9, 2013.

517 Yin, J., Jonkman, S., Lin, N., Yu, D., Aerts, J., Wilby, R., Pan, M., Wood, E., Bricker, J., Ke, Q., Zeng, Z., Zhao, Q., Ge, J.  
 518 and Wang, J.: Flood Risks in Sinking Delta Cities: Time for a Reevaluation?, *Earth's Futur.*, 8(8),  
 519 doi:10.1029/2020EF001614, 2020.

520 Zhai, Y., Yao, Y., Guan, Q., Liang, X., Li, X., Pan, Y., Yue, H., Yuan, Z. and Zhou, J.: Simulating urban land use change by  
 521 integrating a convolutional neural network with vector-based cellular automata, *Int. J. Geogr. Inf. Sci.*, 34(7), 1475–  
 522 1499, doi:10.1080/13658816.2020.1711915, 2020.

523 Zhao, G., Bates, P. and Neal, J.: The Impact of Dams on Design Floods in the Conterminous US, *Water Resour. Res.*, 56(3),  
 524 1–15, doi:10.1029/2019WR025380, 2020.

525 Zhao, L., Song, J. and Peng, Z.-R.: Modeling Land-Use Change and Population Relocation Dynamics in Response to  
 526 Different Sea Level Rise Scenarios: Case Study in Bay County, Florida, *J. Urban Plan. Dev.*, 143(3), 04017012,  
 527 doi:10.1061/(asce)up.1943-5444.0000398, 2017.

528 Zhou, L., Dang, X., Sun, Q. and Wang, S.: Multi-scenario simulation of urban land change in Shanghai by random forest and  
 529 CA-Markov model, *Sustain. Cities Soc.*, 55, 102045, doi:10.1016/j.scs.2020.102045, 2020.

530 Zhou, Q., Leng, G., Su, J. and Ren, Y.: Comparison of urbanization and climate change impacts on urban flood volumes:  
 531 Importance of urban planning and drainage adaptation, *Sci. Total Environ.*, 658, 24–33,  
 532 doi:https://doi.org/10.1016/j.scitotenv.2018.12.184, 2019.

533 Xu, X.: China GDP Spatial Distribution Kilometer Grid Dataset [dataset], <http://www.resdc.cn/DOI/doi.aspx?DOIid=33>,  
 534 2017a.

535 Xu, X.: China Population Spatial Distribution Kilometer Grid Dataset [dataset],  
 536 <http://www.resdc.cn/DOI/DOI.aspx?DOIid=32>, 2017b.